HEFAT2012
9th International Conference on Heat Transfer, Fluid Mechanics and Thermodynamics
16 – 18 July 2012
Malta

STUDY OF INLET PERTURBATIONS ON EXCITATION OF A LAMINAR SEPARATION BUBBLE THROUGH LES

Harish Babu and S. Sarkar*
*Author for correspondence
Department of Mechanical Engineering,
Indian Institute of Technology Kanpur,
Kanpur, 208016,
India,
E-mail: subra@iitk.ac.in

ABSTRACT

A laminar boundary layer over a solid surface occasionally separates under the influence of adverse pressure gradient or sudden change of curvature, undergoes transition due to amplification of the disturbances, becomes turbulent and finally reattaches to form a separation bubble. In this paper, effects of inlet perturbations manifesting free-stream turbulence (*fst*) are examined to highlight the physics of unsteady flow and heat-transfer induced by a change of surface curvature using Large-eddy simulations (LES). Two kinds of inlet perturbations are considered: one case with a deterministic frequency (denoted as case1) and other being a band of frequencies (denoted as case2). The Reynolds number based on inlet velocity and leading edge diameter is 3450. The LES resolves the instability of the separated shear layer and its breakdown forming large- and energetic small-scale structures, which retain their appearance far downstream. When compared with the literature, it suggests that the excitation of boundary layer and thus, history of transition is sensitive to the imposed perturbations, although time-averaged flow characteristics are similar.

Keywords: Separation Bubble, LES, Transition.

INTRODUCTION

A separation bubble is observed close to the leading edge of an airfoil, on a high-lift gas turbine blade and on wings of a micro-aero-vehicle. Presence of the separation bubble deteriorates the performance such as loss of lift with an increase of drag and may act as a source of noise. The schematic of a laminar separation bubble formed over a leading edge is shown in Figure 1 following Ref. 1. The part of the bubble near the separation point contains fluid that is almost stationary. This region is called 'Dead-air' region, which is associated with an almost constant pressure distribution. Near the reattachment point the bubble contains a region of strong re-circulating velocities and can be attributed to the presence of 'Reverse flow' vortex. A strong pressure gradient exists in this region.

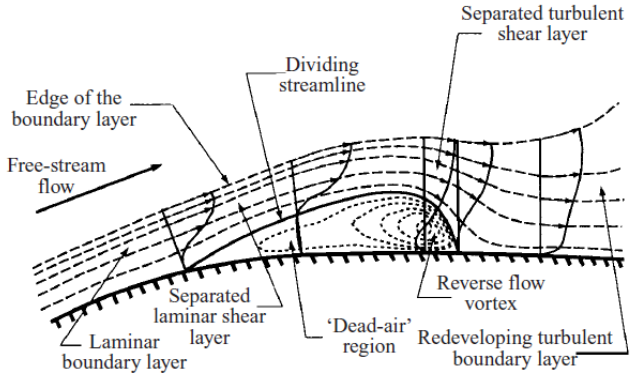

Figure 1 Mean flow structure of a laminar separation bubble following Ref. 1

Many studies were reported illustrating growth of disturbances of a separated shear layer in space and time leading to breakdown. The most notable advancement in the understanding of bubble structure and behaviour came with the work of Gaster [2] illustrating the existence of regions of absolute instability, where the separation was on a flat surface because of pressure gradient. The results of Direct Numerical Simulation (DNS) of laminar separation bubble on a flat plate, where the separation was created by suction applied on the upper boundary is also available in literature [3, 4]. Results of simulation show that the separated shear layer undergoes transition via Λ-vortex-induced breakdown and reattaches as turbulent flow, slowly recovering to an equilibrium turbulent

boundary layer. LES of flow over a blunt leading edge was carried out by Yang and Voke [5]. Their results indicated that the free shear layer formed in the separation bubble is inviscidly unstable and a significant growth of three-dimensional motion is observed in the second half of the bubble, leading eventually to fully turbulent flow around the mean reattachment. Recently, McAuliffe and Yaras [6] performed numerical studies of a separation bubble over a flat plate for two cases: one with an undisturbed free-stream and other with elevated free-stream turbulence. Under low *fst* condition, transition occurs via the Kelvin-Helmholtz (K-H) mechanism, while the path to transition is through transient growth or nonmodal growth for the other case.

In this paper, results from an LES are presented to elucidate the transition, growth of three-dimensional motions and heat-transfer characteristics owing to flow past a semi-circular leading edge for *fst* manifested by two different kinds of imposed inlet perturbations. The Reynolds number based on the leading edge diameter D and inlet velocity U_o is 3450, which is the same as the simulation of Yang and Voke [5]. The objective of the present work was to examine the effect of imposed perturbation on transition of a separated boundary layer apart from resolving the unsteady flow and heat transfer with change of *fst*. The magnitudes of the inlet disturbances were so adjusted that it yields almost the same mean bubble lengths. However, the turbulence intensity evaluated at a point $0.2D$ upstream of the stagnation point along the centre-line at the mid-span were found 0.70% with case1 and 0.36% for case2.

NOMENCLATURE

D	[m]	Leading edge diameter
Cf	[-]	Coefficient of friction
Cp	[-]	Coefficient of pressure
f	[Hz]	Most amplified frequency
fst	[-]	Free-stream turbulence
G	[-]	Clauser parameter
H	[-]	Shape factor
l	[m]	Bubble length
m	[-]	Thwaites parameter
Nu	[-]	Nusselt number
P^+	[-]	Turbulent production kinetic energy, scaled with wall parameters
Pr	[-]	Prandtl number
Re_θ	[-]	Reynolds number based on momentum thickness and local free-stream velocity
St	[-]	Strouhal number, Stanton number
T	[K]	Temperature
T'	[K]	RMS temperature fluctuations
Tu	[-]	Turbulence intensity
U	[m/s]	Velocity component in x-direction
$\bar{u}$	[m/s]	Average velocity
u',v',w'	[m/s]	RMS velocity fluctuations along x,y and z directions respectively
x, y, z	[m]	Cartesian coordinates
$\Delta x^+, \Delta y^+, \Delta z^+$	[-]	Grid spacing in terms of wall units

Special characters

δ	[m]	Boundary layer thickness
δ^*	[m]	Displacement thickness
δ_w	[m]	Vorticity thickness
θ	[m]	Momentum thickness
λ	[-]	Velocity ratio
Λ	[-]	Horton criterion
ν	[m^2/s]	Kinematic viscosity
ω	[-]	Most amplified non-dimensional frequency

Subscripts

e	Local condition
sep	Separation point
max	Maximum
R	Reattachment point
0	Inflow condition

COMPUTAIONAL DETAILS

The three-dimensional unsteady Navier-Stokes equations along with energy equation are solved for Newtonian incompressible flow in Cartesian coordinate system. A dynamic subgrid-scale model proposed by Germano et al. [7] and modified by Lilly [8] is used to model the SGS stress tensor and temperature flux, which represent the effect of subgrid motion on the resolved field of LES. Here, the model coefficient is dynamically calculated instead of input a priori.

The equations are discretized in space using a second order symmetry preserving central difference scheme, which are widely used in LES for their non-dissipative character [9, 10]. The time advancement is explicit using the second-order Adams-Bashforth scheme [11] except for the pressure term, which is solved by a standard projection method. The pressure equation is discrete Fourier transformed in one dimension (in which the flow can be considered homogeneous) and is solved by the BI-CG algorithm in the other two directions [12]. The solver used in the present simulation has been extensively validated for variety of transitional and turbulent flows [13-15]. The details about the solver are available in Ref. 15.

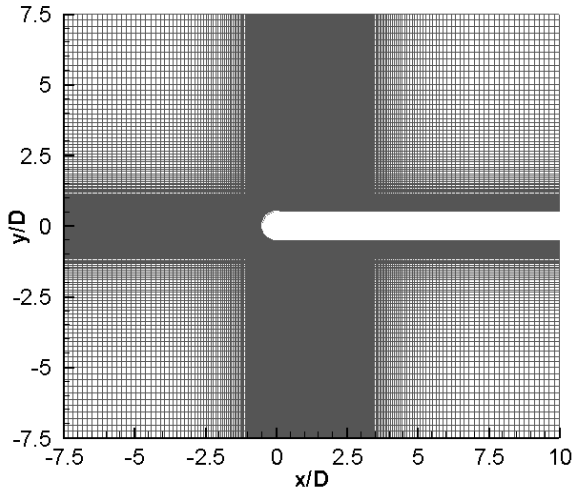

Figure 2: Computational grid and the domain for the semi-circular leading edge.

To resolve the leading edge in Cartesian geometry, the Immersed Boundary (IB) method is used here to apply the boundary conditions, where the geometry is non-conformal to the grid. IB technique used here belongs to the class of 'direct forcing' method [16]. The velocity and temperature field near the boundary of the body is modified at each step in such a way

that the no-slip boundary condition and the constant temperature wall are satisfied. This is done using an interpolation technique, which is equivalent to including a body force in the momentum and energy equations. In the present simulation, the quadratic unidirectional interpolation technique is used [15, 17].

Figure 2 depicts the computational domain and the mesh. The origin of the computational domain is the centre of the semicircular leading edge. The streamwise, wall normal and spanwise direction are the x, y and z directions, whereas, the corresponding velocity component are u, v and w. The domain extends form -7.5D to 10.0D in the streamwise direction, -7.5D to 7.5D in the flow normal direction. The z-span used in the simulation is 2.0D. A previous study on boundary layer separation using similar geometry at same Reynolds number reported that a length of 2D in the z-direction was sufficient to resolve the flow structure [5]. Free-stream boundary condition is imposed at the top and bottom boundary of the computational domain. At the inlet, the inflow velocity is considered as uniform and parallel to the plate, while a convective boundary condition is taken at the outflow boundary. The spanwise direction is taken to be periodic. The grid in z-direction is uniform, while non-uniform grid distributions are used in the x and y directions with finer resolution in the vicinity of body to resolve the boundary layer. A mesh refinement test was carried out and a mesh of 304×224×64 in the streamwise, wall normal and spanwise directions was chosen. A sub domain of size 3.7D×3.0D near the leading edge is considered, where a refined mesh is used to properly resolve the flow using IB method. A total of 161×184 grid points are employed inside this region. Away from the body surface in crosswise and in streamwise direction the meshes are slowly stretched out and finally a uniform grid is employed. The near wall resolution in a region x/D =0.0-3.0, y/D=0.0-0.5 (from the surface) is $2.5 < \Delta x^+ < 5.5$, $1.2 < \Delta y^+ < 5.25$ and $3.0 < \Delta z^+ < 7.0$.

RESULTS AND DISCUSSIONS

MEAN FLOW CHARACTERISTICS

The variations of coefficient of skin friction C_f as a function of distance (normalized with respect to leading edge diameter) from blend point for the two cases considered are shown in Figure 3. The initial flat portion after the separation point corresponds to the dead air region of the bubble, whereas, the reverse flow vortex region is associated with a much larger negative skin friction. The separation and reattachment points are located by zero crossing of C_f plots. The time averaged bubble length in the experiment was about 2.75D for an *fst* less than 0.2% [18]. In the present LES, a bubble length of 2.78D was obtained for case1, whereas, the bubble length was 2.82D for case2.

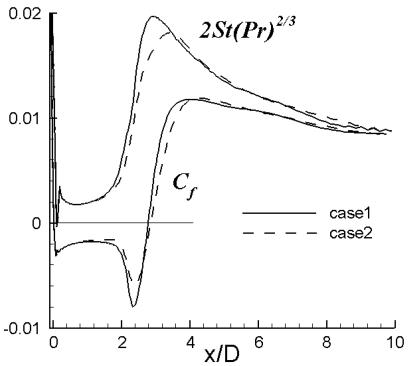

Figure 3 Variation of C_f and St for the separation bubble

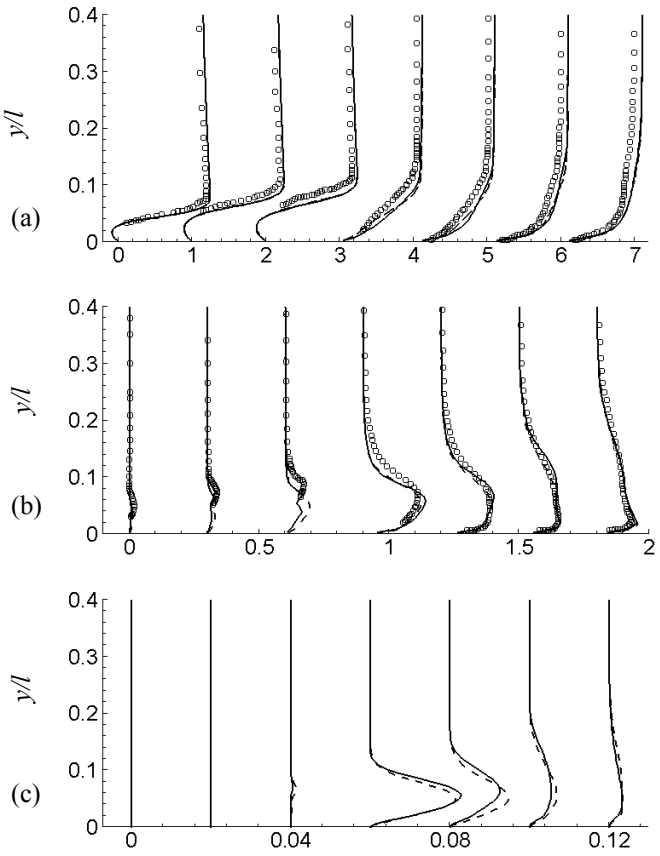

Figure 4 (a) Mean streamwise velocity, (b) r.m.s. streamwise velocity fluctuation u', (c) Reynolds stress $-\langle u'v' \rangle$, computed at seven streamwise locations measured from the blend point at x/l = 0.22, 0.44, 0.66, 1.09, 1.27, 1.64, 2.55. ———, case1; - - - - -, case2, ○○○ experimental data.

To illustrate the evolution of heat transfer in the separated boundary layer, the distribution of Stanton numbers (St) is superimposed on the C_f distribution. A factor of $2Pr^{(2/3)}$ is used for flow and heat transfer analogy, where Pr denotes prandtl number [19]. This widely used analogy is based on experimental data for both laminar and turbulent flows. The Stanton number becomes maximum at the point where the Cf

is minimum, which corresponds to the breakdown of shear layer. As downstream is approached $2StPr^{(2/3)}$ slowly drops down and approaches the value of C_f illustrating an equilibrium boundary layer.

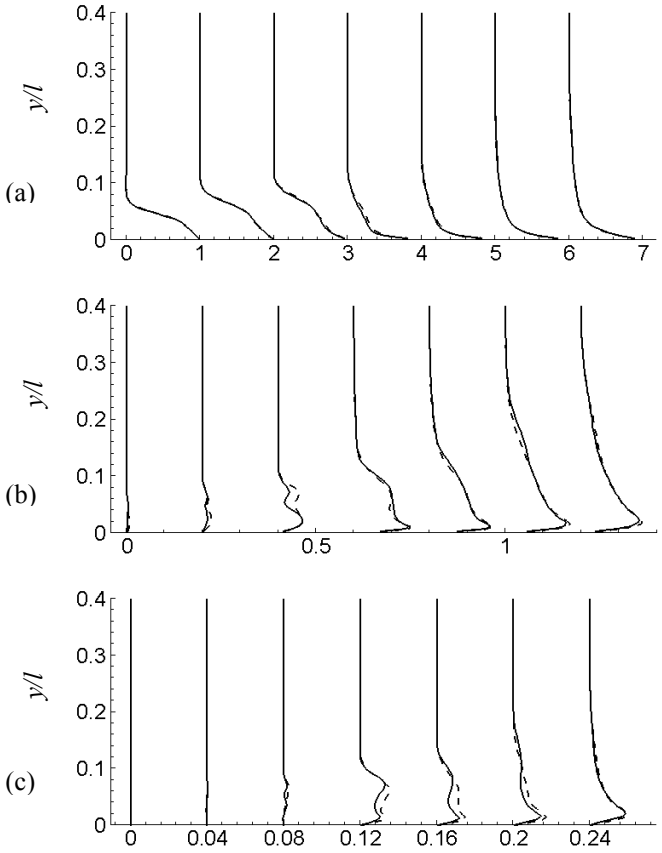

Figure 5 (a) Mean Temperature, (b) r.m.s. temperature fluctuation T', (c) Turbulent heat flux $-\langle u'T' \rangle$, computed at seven streamwise locations measured from the blend point at *x/l* = 0.22, 0.44, 0.66, 1.09, 1.27, 1.64, 2.55. ———, case1; - - - - -, case2,

The mean streamwise velocity and rms. fluctuation along the streamwise direction are compared with the experimental data of Coupland and Brierley [18] at seven streamwise locations, Figure 4a-b. The profiles are plotted as a function of y/l at different values of x/l, where, l is the mean bubble length. The origin for the plots has been chosen at the top blend point, where the leading edge joins the flat plate. In these figures, the profiles are arbitrarily shifted on horizontal axis to represent the variation of flow variables with respect to the change in position along the streamwise direction. There is not much change in the mean streamwise velocity profile for the two types of imposed perturbations. The match with the experimental results is also good. The profile approaches an equilibrium profile at the last station. There are some minor differences in the rms fluctuations for the two cases, especially at the second and third station. The main difference is that for case1 a double peak structure is seen, while for case2, it shows only a single peak. Experimental results are also not available near the wall for these stations.

The magnitude of u' begins to increase in the shear layer after separation. The peak in u' occurs in the outer layer for streamwise locations inside the bubble, while the peak is shifted towards the wall after reattachment. Just downstream of separation, the increase in u' occurs with an almost zero value of turbulent stress $-\langle u'v' \rangle$, which indicates that the shear layer is laminar. As flow proceeds downstream, non-zero values of $-\langle u'v' \rangle$ appear in the second half of the bubble. For locations just downstream of reattachment, the peak values of $-\langle u'v' \rangle$ is well away from the wall, indicating a high active outer layer, that is generally being observed for a separated layer. It has also been seen that the reattached turbulent boundary layer slowly approaches to an equilibrium condition far downstream. The two kinds of perturbation have resulted in almost similar time averaged characteristics of the separated layer and the results are consistent with those reported earlier [20].

The mean temperature profiles are plotted in Figure 5a and r.m.s. value of its fluctuations (T') in Figure 5b. The mean temperature profile like the velocity profile does not show any appreciable difference for the two cases. The high near wall temperature after reattachment is because of dissipation. However, higher values of T' fluctuations with double peak are seen in the outer layer for case2 compared to case1 within the separated region. The fluctuations in the outer layer die down as the flow proceeds downstream with development of a peak near the wall. Similar effect is seen in the turbulent heat fluxes $-\langle u'T' \rangle$ (Figure 5c), depicting high values in the shear layer near reattachment. This illustrates significant turbulent heat flux from the wall because of breakdown of bubble and formation of large-scale vortices. After reattachment, the near wall heat flux predominates illustrating an equilibrium layer. It should be noted that there are difference in minute details in profiles of T' within the separation bubble and $-\langle u'T' \rangle$ after reattachment, which is consistent with u' and $-\langle u'v' \rangle$.

The distribution of surface pressure coefficient (C_p) along the streamwise direction is shown in Figure 6. It can be seen that the location of the bubble corresponds to a region of strong adverse pressure gradient. The adverse pressure is found to exist a short distance downstream of reattachment, followed by a favourable pressure gradient. The time-averaged surface characteristics when non-dimensionalised with bubble length are found to be similar for the two imposed inlet perturbation.

Figure 7 plots the variation of boundary layer displacement thickness, momentum thickness and shape factor for the two imposed inlet disturbances. The shape factor reaches maximum value at start of transition [21]. It can be seen that shape factor is maximum at *x/l* = 0.56 irrespective of type of perturbation imposed. The value of shape factor at reattachment is found to be 3.13 and 3.82 for case1 and case2 respectively. This is close

to the value 3.5 predicted by Horton [22]. H is found to reach an asymptotical value of 1.6, which is close to the value 1.3-1.4 taken as the shape factor for turbulent flow over a flat plate with no pressure gradient. The momentum thickness starts growing after *x/l* = 0.7 and becomes maximum after reattachment illustrating augmentation of turbulence due to breakdown and formation of large-scale vortices.

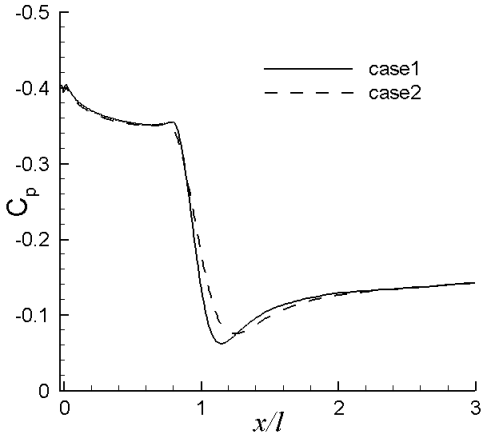

Figure 6 Variations of Cp in streamwise direction

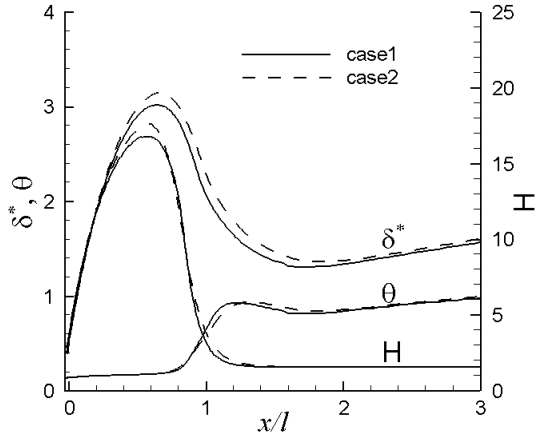

Figure 7 Variations of boundary layer integral parameters

Separation criterion based on the parameter *m* has been reported in literature. The parameter *m* is based on flow conditions at separation and is calculated as

$$m = \frac{\theta_{sep}^2}{\nu}\left(\frac{dU_e}{dx}\right)_{sep}$$

Curle & Skan [23] found -0.171 < *m* < -0.068 for the onset of separation, while Thwaites [24] suggested *m* = -0.08. In the present simulations, *m* was found to be -0.072 and -0.073 for case1 and case2 respectively, which are within the limits [23]. Another integral parameter is the Horton's criterion at reattachment defined as

$$\Lambda_R \equiv \left[\frac{\theta}{U_e}\frac{dU_e}{dx}\right]_R$$

The suggested value of which is -0.0082 [22] and was later modified [25] to -0.0059. In the present simulation, the value of this parameter was found to be -0.0024 and -0.0031. The difference in the values may be appreciated because boundary layer separation in the present case is induced by the leading edge curvature. It should be noted that Horton's or Thwaites criterion for separation is derived neglecting the effect of surface curvature.

INSTABILITY ANALYSIS

The necessary and sufficient condition for flow to be unstable via invisid instability is the presence of an infection point in the velocity profile. From Figure 4(a), it can be seen that the velocity profiles have an infection point and are hence invisidly unstable. A detailed instability analysis follows.

Similar to a mixing layer, a free shear layer between two streams of velocities U_1 and U_2 has two velocity scales: the velocity difference $\Delta u = |U_1 - U_2|$ and the average velocity $\bar{u} = (U_1 + U_2)/2$. Vorticity thickness $\delta_w = \Delta u/(du/dy)_{\max}$ may be used as the characteristic length scale. The velocity difference across the shear layer is characterised by the factor velocity ratio $\lambda = \Delta u/(2\bar{u})$. The most amplified non-dimensional frequency $\omega_{\max} = \left(\frac{1}{4}\delta_w\right)(2\pi f/\bar{u})$ is almost constant (0.222 to 0.21) for a wide range of λ (0 to 1). In the present study, $\omega_{\max}$ is found to occur within the above limits at various streamwise locations for the two cases. The close agreement between the theoretical and experimental results indicates that the flow is unstable via inviscid instability mechanism.

It has been shown that the flow is absolutely unstable for reverse flow is greater than 15% [3]. For the current simulations, the maximum reverse flow is found to be less than 10% in the regions where transition initiates and hence it can be concluded that there are no regions of absolute instability.

INSTANTANEOUS FLOW STRUCTURES:

Figure 8 and 9 shows the instantaneous temperature contours: (*a*) in the side view (*x*-*y* plane) at mid-span and (*b*) in the top view (*x*-*z* plane) at *y* = 0.04*D* from top wall. The contours of instantaneous temperature illustrate the internal growth mechanism of shear layer and formation of three-dimensional flow structures under excitation of the two kinds of inlet perturbations. The temperature contours in the *x*-*y* plane (side view), illustrates that the instability of the separated shear layer is attributed to the enhanced receptivity to perturbations forming K-H rolls that break down near reattachment. Both the perturbations have resulted in similar effect evolving shedding of large-scale vortices that retain their identity far downstream.

The difference in excitation is more appreciable in the *x-z* plane (top view) for a wall normal location of y/D = 0.04. Three-dimensional motions sets in downstream of x/l = 0.3, followed by appearance of longitudinal streaks, the characteristics of transition. These streaks undergo elongation and breakdown near the reattachment forming small scale eddies. It is interesting to note that the spanwise characteristics of these streaks in the shear layer are different with inlet perturbation with a band of frequencies. In this case, the small scale eddies are abundant as compared with the imposed inlet perturbation having a deterministic frequency.

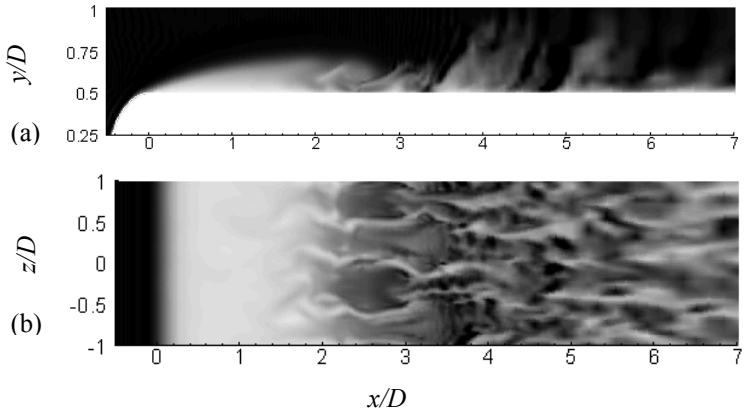

Figure 8: Instantaneous flow structures for case1 (imposed perturbations having a deterministic frequency)

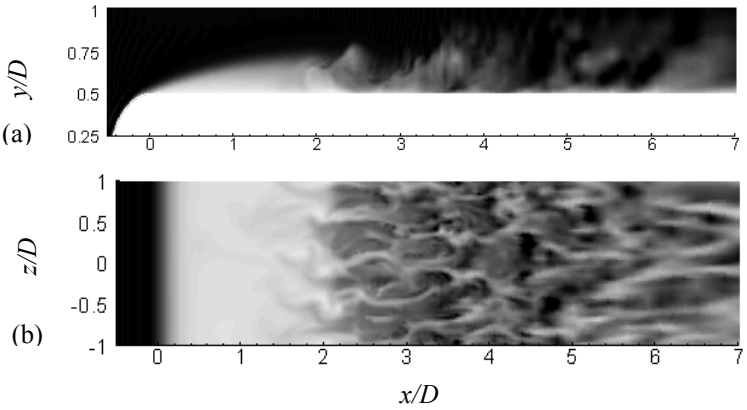

Figure 9: Instantaneous flow structures for case2 (imposed perturbations having a band of frequencies)

TURBULENCE SPECTRA

It has been seen that the shedding process from a separated shear layer seems to happen within a range of frequencies rather than with a single frequency. The shedding frequency may be non-dimensionalized using the momentum thickness and local free stream velocity at separation to get the Strouhal number (*St*). The reported values of *St* are 0.0068 [26], 0.005 to 0.011 [5], 0.011 [6] to mention a few. In addition, a low frequency flapping corresponding to *St* = 0.001 has also been observed [5, 27]. It was explained in Ref.5 that during normal vortex shedding, small bubbles are ejected from the tail of a big separation bubble resulting in a slight change in the instantaneous reattachment point. However, the small bubbles may occasionally coalesce and then eject from the separation bubble resulting in a low frequency flapping and large reduction in the reattachment point.

The spectra of velocity fluctuation for the two different kinds of imposed perturbations at y/l = 0.04 and mid-span are shown in Figure. 10 and 11 for the stations x/l = 0.0 to 1.2 in steps of 0.1, 1.5, and 2.0. The power spectral density (*PSD*) has been shifted by an arbitrary amount in the vertical axis.

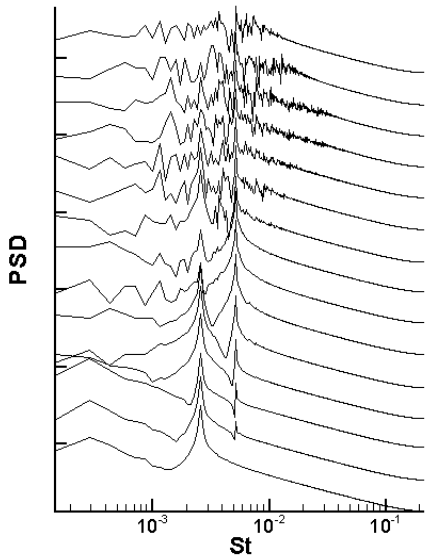

Figure 10 Spectra of velocity fluctuation for case1 (imposed perturbations having a deterministic frequency)

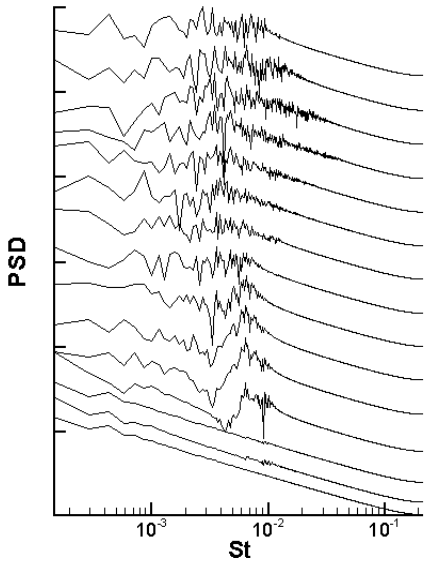

Figure 11 Spectra of velocity fluctuationfor case2 (imposed perturbations having a band of frequencies)

For case1 (imposed inlet perturbations with single frequency), the vortex shedding is dominated by the imposed frequency and its harmonic, which is twice the imposed frequency. This can be noted from very beginning of the bubble. The peak occurs at imposed frequency till x/l = 0.4 and then further downstream its harmonic becomes predominant and the amplitudes being comparable. It should be noted that the harmonic when non-dimensionalised (St = 0.0055) falls within the range 0.005 – 0.011. However, at x/l = 0.8 and beyond, a wide range of frequencies (St = 0.0015 to 0.015) are apparent with can be attributed to the breakdown of shear layer. However, even far downstream the existence of the imposed frequency and its harmonic prevail, illustrating the fact that the shear layer instability and the shedding process is highly influence by the inlet imposed frequency of perturbation.

What is revealing to note is that for case2 (imposed inlet perturbations with wide range of frequencies), no perturbations are observed up to x/l = 0.2 depicting that the flow is laminar in the beginning of separation. At x/l = 0.3 and beyond, the vortex shedding is not periodic with a single frequency, rather the shedding process occurs with a wide range of frequencies, St = 0.005-0.011, which is the same as reported earlier by Yang and Voke [5]. The averaged frequency can be estimated to be about St = 0.008. In addition, there is also a peak at St = 0.001, which indicates the occurrence of low frequency flapping. At x/l = 0.3 to 0.5, the frequency corresponding to maximum amplitude is at St = 0.00686, which is close to the value obtained in simulation by Pauley et al [26]. Between x/l = 0.7 - 0.8, breakdown occurs with a wide range of frequencies (St = 0.0015 to 0.019) indicating appearance of energetic small scale eddies. The relatively wider spectra with band of frequencies which has been resolved can be correlated with the abundant small scale eddies present in the instantaneous flow structures Figure 9.

The history of flow and the path of succession through which transition and breakdown occur appear more natural for case2 compared to case1. Thus, although the time-averaged characteristics become independent of imposed perturbations, the path of succession through which transition occurs is influenced by imposed perturbations. Thus, the more realistic flow features will be resolved if a proper inlet perturbation is imposed. A model of imposed perturbation that properly mimics free-stream disturbance in wind tunnel is needed to resolve the transitional flow. Caution should be taken while resolving the transitional flow with imposed perturbations having a single frequency.

BOUNDARY LAYER RELAXATION

The Clauser parameter defined as $G = \left(\frac{H-1}{H}\right)\sqrt{\frac{2}{C_f}}$ is plotted as a function of $\left(x - x_R\right)/\delta_R$ in Figure 12. Both the inlet disturbances have resulted in similar trend. The boundary layer relaxation approaching to equilibrium can be appreciated by the Clauser parameter [3]. Flat plate boundary layer with zero pressure gradient has an equilibrium value of G = 6.8. However, in the present work, the flow is past a semi-circular leading edge and hence experiences a non-zero pressure gradient. Thus, the departure of the values of Clauser parameter from 6.8 in the present case may be attributed to the concerned flow environment. It appears that the boundary layer relaxation is slow and recovery length to reach a fully equilibrium layer would require much longer computational box. Similar observation was also noted while studying the boundary layer relaxation from a laminar separation bubble [3].

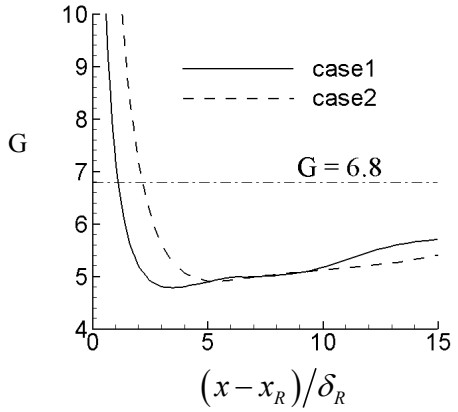

Figure 12: Boundary layer development after reattachment

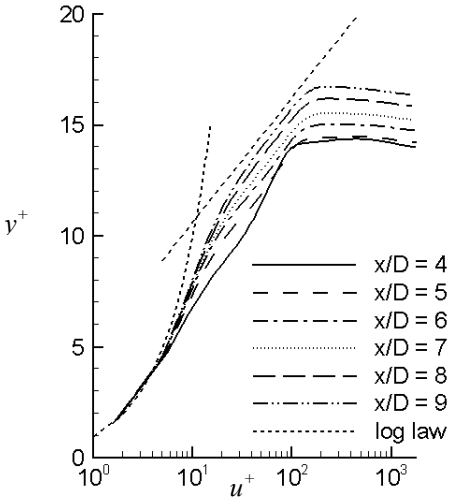

Figure 13: Boundary layer development after reattachment for case1 (imposed inlet perturbations with single frequency)

The velocity profile for case2 at different streamwise locations is compared with the log-law velocity profile. A slow relaxation of the profile to the log-law profile is observed with the velocity profile always lagging below the log law profile. A similar trend is also observed for case1. It should be noted that there is considerable difference between the turbulent boundary layer profile just downstream of reattachment and a canonical layer. It takes at least seven times the bubble length to reach an equilibrium layer [3]. Castro and Epik [28] have shown that the recovery length of attached turbulent boundary layer to reach

equilibrium is more than 75 times boundary layer thickness at reattachment.

To characterise the state of boundary layer after reattachment, the profiles of the time-averaged turbulent production kinetic energy (scaled with wall parameters) $P^+ = -\overline{u'v'}^+ \left(dU^+/dy^+\right)$ for different streamwise locations are compared with DNS [30] and experimental data of [29] in Figure 14.

In Ref 30, it was shown that profiles of *P*+ of a turbulent layer at three different momentum thickness Reynolds number (Re_θ = 300, 670, 1410) are self-similar. *P*+ evaluated from the resolved part of the present LES reproduce the feature of almost self-similarity in profiles downstream of *x/D* = 5, although the data of Kim et al [29] and Spalart [30] are under predicted by 14%. It should be also noted that the value of Re_θ calculated from the present LES is approximately 210-260 in the range at *x/D* = 5 – 9. The boundary layer becoming turbulent in the range of relatively low range of Re_θ: characteristics of separation induced transition.

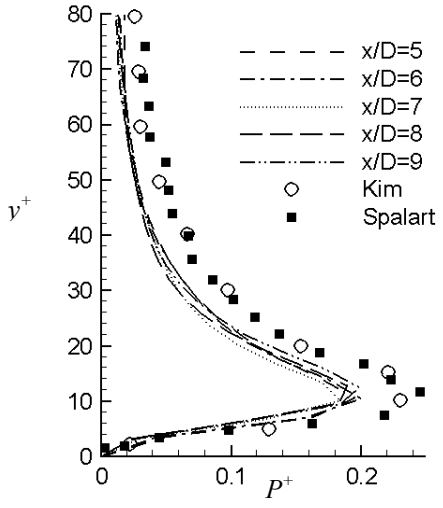

Figure 14: PKE after reattachment for case1 (imposed inlet perturbations with single frequency)

CONCLUSION:

To examine the excitation of a laminar separation bubble under the influence of free-stream turbulence, two different kinds of inlet perturbations are imposed: one with a deterministic frequency and other having a band of frequencies. To compare their relative effect, the amplitude of the disturbances are so adjusted that it results in almost the same mean bubble length in both the cases. The LES resolves the instability of separation bubble and its breakdown via KH mode resulting in large and small-scale energetic structures.

It is interesting to note that the non-linear growth of perturbations during the succession of transition is strongly influenced by the imposed inlet perturbations and its frequency. The spectra of velocity fluctuations show remarkable difference during first half of the separated layer indicating that the transition and vortex shedding depend on the inlet disturbances. The path of succession through which transition and breakdown occurs appear more realistic for the imposed perturbations containing a band of frequencies. However, after breakdown, the time-averaged turbulence characteristics such as stresses, heat flux tensor and also integral parameters are almost indistinguishable. Some minor differences can be appreciated in turbulent heat flux and stresses in the second half of the bubble and near reattachment. Further, the spanwise spacing of transition streaks in the shear layer are different with different inlet perturbations, resolving abundant small scale eddies apart from large coherent structures for the inlet perturbation having a band of frequencies as compared with a deterministic frequency.

Thus for a laminar separation bubble, the excitation of the separated layer and transition depends on proper inlet boundary conditions reflecting the free-stream turbulence, but after breakdown the time-averaged turbulence flow characteristics is not sensitive to the nature of inlet perturbations.

REFERENCES:

[1] Horton, H. P. Laminar separation in two and three-dimensional incompressible flow, PhD Dissertation, University of London, 1968

[2] Gaster, M., Structure and behaviour of laminar separation bubbles, ARC R&M 3595, HMSO, 1969

[3] Alam, M. & Sandham, N. D., Direct numerical simulation of 'short' laminar separation bubbles with turbulent reattachment, *Journal of. Fluid Mechanics,* Vol. 410, 2000, pp. 1-28

[4] Spalart, P.R., Strelets, M.K.H., Mechanism of transition and heat transfer in a separation bubble, *Journal of Fluid Mechanics*, Vol. 403, pp. 329–349, 2000.

[5] Yang, Z.Y. & Voke, P.R., Large eddy simulation of boundary layer separation and transition at change of surface curvature, *Journal of Fluid Mechanics*, Vol. 439, 2001, pp. 305–333, 2001.

[6] McAuliffe, B. R., Yaras, M. I., Transition Mechanisms in Separation Bubbles under Low and Elevated Free-stream Turbulence, *Journal of Turbomachinery*, Vol. 132, 2010,pp 011004-1 - 011004-10

[7] Germano, M., Piomelli, U., Moin, P., Cabot, W. H., A dynamic subgrid-scale eddy viscosity model, *Physics of Fluids A*, Vol. 3, 1991,pp. 1760-1765.

[8] Lilly, D.K., A proposed modification of the Germano subgrid-scale closure method, *Physics of Fluids A*, Vol. 4, 1991, pp. 633-635.

[9] Mittal, R., and Moin, P., "Suitability of Upwind-Biased Finite-Difference Schemes for Large-Eddy Simulation of Turbulent Flows," *AIAA Journal*, Vol. 35, 1997, pp. 1415–1417.

[10] Morinishi, Y., Lund, T. S., Vasilyev, O. V., and Moin, P., Fully Conservative Higher Order Finite Difference Schemes for Incompressible Flow, *Journal of Computational Physics,* Vol. 143, 1998,pp. 90–124.

[11] Chorin, A. J., Numerical solution of the Navier–Stokes equations, *Mathematics of Computation*, Vol 22, 1968, pp. 745–762.

[12] Zhang, S. L., GPBI-CG: Generalized product-type methods based on Bi-CG for solving nonsymmetric linear systems, *SIAM Journal of Scientific Computation*, Vol. 18, 1997, pp 537-551.

[13] Sarkar, S., Identification of flow structures on a LP turbine blade due to periodic passing wakes, *ASME Journal of Fluids Engineering*, Vol. 130, 2008, 061103.

[14] Sarkar, S., Influence of wake structure on unsteady flow in an LP turbine blade passage, *ASME Journal of Turbomachimery*, Vol. 131, 2009,041016.

[15] S. Sarkar and Sudipto Sarkar, Large-Eddy Simulation of Wake and Boundary Layer Interactions Behind a Circular Cylinder, *ASME Journal of Fluids Engineering,* Vol. 131,2009, 091201.

[16] Fadlun, E. A., Verzicco, R., Orlandi, P. and Mohd.-Yusof, J., "Combined immersed boundary finite difference methods for three dimensional complex flow simulations, *Journal of. Computational Physics,* Vol. 161, 2000, pp. 35-60.

[17] Muldoon, F. and Acharya, S, 2005, Mass conservation in immersed boundary method, Proceeding *of FEDSM 2005,* FEDSM-77301, pp. 1-9.

[18] Coupland, J., Brierley, D., 1996, "Transition in turbomachinery flows," Final Report, BRITE/EURAM Project AERO-CT92-0050.

[19] Colburn, A. P. A method of correlating forced convection heat transfer data and a comparison with fluid friction. *Transactions of the American Institute of Chemical Engineers*, Vol. 29, 1933, pp. 174-210.

[20] Volino, R. J., Separated Flow Transition Under Simulated Low-Pressure Turbine Air-Foil Conditions: Part 1—Mean Flow and Turbulence Statistics, *ASME Journal of Turbomachimery*, Vol. 124, 2002, pp. 645–655.

[21] Ellsworth, R.H., Mueller, T.J. Airfoil boundary layer measurements at low Reynolds in an accelerating flow from a nonzero velocity. *Experiments in Fluids,* Vol. 11, 1991, 368–374.

[22] Horton, H. P. 1967 A semi-empirical theory for the growth and bursting of laminar separation bubbles. Aeronautical Research Council, CP1073.

[23] Curle, N., and Skan, S. W. Approximate methods for predicting separation properties of laminar boundary layers. *Aero.Q*. Vol. 8, 1957, 257-268.

[24] Thwaites B, Approximate calculation of the laminar boundary layer. *Aero.* Vol Q. Vol. 14, 1949, pp. 61-85.

[25] Roberts, W. B. 1980 Calculation of laminar separation bubbles and their effect on aerofoil performance. AIAA J. Vol 18, 25-31.

[26] Pauley, L. L., Moin, P. & Reynolds, W. C., The structure of two-dimensional separation, *Journal of Fluid Mechanics*, Vol. 220, 1990 pp. 397-411.

[27] Cherry, N. J., Hillier, R. & Latour, M. P., Unsteady measurements in a separated and reattaching flow, *Journal of. Fluid Mechanics,* Vol. 144, 1984, pp. 13-46.

[28] Castro, I. P. & Epik, E. Boundary-layer relaxation after a separated region. *Experimental Thermal and Fluid Science,* Vol. 13, 1996, pp 338 - 348.

[29] Kim, H. T., Kline, S. J., and Reynolds, W. C., An Experimental Study of Turbulence Production Near a Smooth Wall in a Turbulent Boundary Layer With Zero Pressure Gradient, Stanford University, CA, Report No. MD-20, 1968.

[30] Spalart, P. Direct simulation of a turbulent boundary layer up to $Re_\theta = 1410$. *Journal of Fluid Mechanics,* Vol. 187, 1988, pp 61-98.